Synthesis and Luminescence Properties of Nano-/Microstructured Y3Al5O12:Ce3+ Microspheres by Controlled Glass Crystallization

5 AUTHORS, INCLUDING:

Gang He
Chinese Academy of Sciences
19 PUBLICATIONS **76** CITATIONS

SEE PROFILE

Guanghua Liu
Technical Institute of Physics and Chemistry
98 PUBLICATIONS **548** CITATIONS

SEE PROFILE

Synthesis and Luminescence Properties of Nano-/Microstructured Y$_3$Al$_5$O$_{12}$:Ce^{3+} Microspheres by Controlled Glass Crystallization

Gang He,[†,‡] Lin Mei,[†,‡] Lili Wang,[§] Guanghua Liu,[†] and Jiangtao Li*[,†]

[†]Technical Institute of Physics and Chemistry, Chinese Academy of Sciences, Beijing 100190, China
[‡]Graduate School of the Chinese Academy of Sciences, Beijing 100039, China
[§]Department of Materials Science and Engineering, University of Science & Technology Beijing, Beijing 100083, China

ABSTRACT: Nano-/microstructured Y$_3$Al$_5$O$_{12}$:Ce^{3+} microspheres have been successfully synthesized by a controlled glass crystallization method. Glass microspheres were first prepared via a flame spraying—water quenching technique, and then subsequent heat-treatment was used to control the crystallization. The effect of the heat-treatment temperature on the structural and morphological evolution of Y$_3$Al$_5$O$_{12}$:Ce^{3+} microspheres has been investigated. It was found that the as-obtained microspheres composed of randomly aggregated crystallites and their size can be tuned from nanometer scale to micrometer size by adjusting the heat-treatment temperature. The activation energy is 578 ± 16 kJ/mol for crystallization of the glass microspheres, and the crystallization mechanism has been proposed as homogeneous crystallization. The photoluminescence and photoluminescence excitation spectra, the luminescence decay curve, and the effects of heat-treatment temperature and different fluxes on luminescence properties were investigated in detail. The reported method for synthesizing nano-/microstructured microspheres provides a great opportunity for evaluating the luminescence properties of Y$_3$Al$_5$O$_{12}$:Ce^{3+} phosphor.
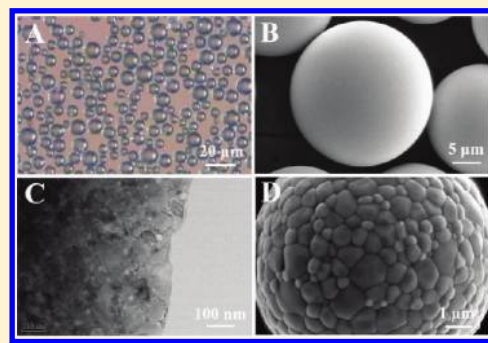
1. INTRODUCTION

White light emitting diodes (LEDs) are considered as the next-generation lighting source for general illumination because of their high efficiency, long lifetimes, and environment friendliness compared to conventional incandescent lamps and fluorescent lamps.[1−3] To generate white light from LEDs, strategies involve combining several LED chips of different colors or using phosphors to downcovert the emission from a blue or ultraviolet LED.[4−6] Among them, coating of a yellow-emitting phosphor on a InGaN blue LED is widely produced due to the easy fabrication and low cost associated with this combination.[7,8] At present, cerium doped yttrium aluminum garnet Y$_3$Al$_5$O$_{12}$:Ce^{3+}(YAG:Ce^{3+}) is the most widely used yellow phosphor in white LEDs. The luminescent properties of phosphor particles are highly affected by the geometrical factors, such as size and shape.[9] The ideal morphology of phosphor particles includes a perfect spherical shape, narrow size distribution, and nonagglomeration. A spherical morphology is good for high brightness because high packing densities and low light scattering can be obtained by using it.[10,11] However, commercial YAG:Ce^{3+} phosphor particles synthesized by conventional solid-state reaction often have agglomerated and irregular shapes and larger sizes. So far, many methods have been developed to control the spherical shape, size, and distribution of phosphor particles, such as spray pyrolysis,[12,13] a sol—gel process,[14] and a coprecipitation method.[15]

Phosphor particles always show unique shape- and size-dependent properties.[16−18] Recently, some attention has been paid to the design and synthesis of nano-/microstructured phosphor particles with well-defined morphologies and accurately tunable sizes, such as

flower-like YVO$_4$:Eu^{3+} superarchitectures,[19] pompon-shape NaGdWO$_4$(OH)$_x$:Eu^{3+} microarchitectures,[20] Y$_2$O$_3$:Eu^{3+} microspheres, and microcubes.[21] These phosphor particles have complex three-dimensional (3D) architectures assembled by nanostructured building blocks such as nanoplates, nanoparticles, nanoribbons, and nanorods.[19,22] The synthesis of those nano-/microstructured micromaterials not only solves the problem of nanoparticles agglomeration but also makes it possible to improve the properties of existing materials. To date, many methods have been developed to synthesize nano-/microstructured materials, including microemulsion, a hydrothermal method, a supercritical solvothermal method, a gel combustion method, and so on.[23−27] However, it is still attractive to develop simple and reliable synthetic methods for nano-/microstructured phosphors with controlled particle size and spherical morphology. Controlled glass crystallization is a well-known method of synthesizing nanocrystalline glass-ceramic materials to control grain growth.[28−30] Typically, the glass matrix is prepared by melting and then subjecting to a controlled heat-treatment to obtain the desired grain sizes.[31,32] However, to the best of our knowledge, few studies have focused on the synthesis of spherical nano-/microstructured YAG:Ce^{3+} particles through a controlled glass crystallization method. This should be correlated to the fact that oxide melts lacking conventional glass-formers are prone to crystallization during slow cooling. To form glass, they must be kinetically frozen by rapid quenching.[33,34] Rosenflanz et al.[34] have shown that glass

microspheres with eutectic compositions of alumina-rare-earth oxide systems (Al_2O_3-RE_2O_3) can be prepared at cooling rates less than 10^3 K/s by a flame spraying—water quenching technique, and fully dense bulk glasses have been obtained through viscous sintering of glass microspheres. It is expected that glass microspheres of YAG composition could also be prepared by a flame spraying—water quenching method, though it is not a eutectic composition. Thus, the nano-/microstructured YAG:Ce^{3+} microspheres could be synthesized by crystallizing the rapidly quenched glass microspheres.

In this paper, we report the preparation of nano-/microstructured YAG:Ce^{3+} microspheres via a controlled glass crystallization method. The glass microspheres were first prepared by a flame spraying—water quenching technique and then subsequently heat-treated to obtain the desired nano-/microstructures. The phase structure, morphology, crystallization mechanism, and luminescence properties of the as-synthesized nano-/microstructured YAG:Ce^{3+} microspheres have been investigated in detail.

2. EXPERIMENTAL SECTION

2.1. Preparation. The rare earth oxides Re_2O_3 (Re = Y,Ce) (99.99%) and Al_2O_3 (99.99%) were purchased from China Minmetals (Beijing) Research Institute, and other chemicals were purchased from Bejing Chemical Reagent. All chemicals were analytical grade reagents and were used directly without further purification. The starting powders were blended together according to the stoichiometric ratio of $(Y_{2.94}Ce_{0.06})Al_5O_{12}$ and were ball-milled with high-purity Al_2O_3 balls for 12 h in distilled water, with 1.0 wt % polyvinyl alcohol (PVA) as an adhesive. The solid content of the all aqueous suspensions was maintained at 50 wt %. The milled aqueous suspension was spray dried with a laboratory spray drier (B-290, BÜCHI, Switzerland). The aqueous suspension was pumped at a flow rate of 10 mL/min with the atomizing air flow rate set at 660 L/h through a 1.4 mm diameter nozzle. The inlet and the outlet temperatures were set at 200 and 120 °C, respectively. The spray-dried powders were calcined at 600 °C for 2 h in air to remove the residual organic components. The as-calcined powders were fed into a oxygen-acetylene gun (ZB-F6P, Beijing Aerospace Zhenbang, China) with a powder feeder at a rate of 10 g/min using an argon carrier gas. The flow rates of acetylene (C_2H_2) and oxygen (O_2) were 15 and 20 L/min, respectively. The high temperature oxygen-acetylene flame (>3000 °C) was vertical to the water surface with a distance of 200 mm. The as-calcined powders that dispersed and fused in the oxygen—acetylene flame were rapidly quenched in water at an estimated cooling rate of 10^3 K/s to retain an amorphous state. The raw powder deposited at the bottom of the water container was collected, washed with distilled water, and dried. The dried raw powder was heat-treated at selected temperatures from 900 to 1500 °C for 4 h (heating rate is 5 °C/min) in a reducing atmosphere of H_2 (5%) and N_2 (95%).

2.2. Characterization. Phase identification of the raw powder and heat-treated samples was characterized by powder X-ray diffraction (XRD,D8 Focus, Bruker, Germany) with Cu Kα radiation (λ = 0.15405 nm) and a scanning speed of 6° per minute. Fourier transform infrared spectra of the raw powder and heat-treated samples were measured in the range 4000−400 cm^{-1} using the KBr pellet ($\sim$1 wt % sample) method with a Nicolet IR200 spectrometer (FTIR, Nexus470, Nicolet, MA). Each analysis consisted of a minimum of 32, scans and the resolution was $\pm$2 cm^{-1}. Morphologies of the samples were observed via scanning electron microscopy (SEM, Hitachi S-4300, Japan), transmission electron microscopy (TEM, JEOL-2010, 200 kV), and optical microscopy (Leica, DM-1000, Germany). The specimen was prepared by spreading the powders on the carbon seals for SEM. For TEM preparation the powder sample was mixed with a fine Cu powder
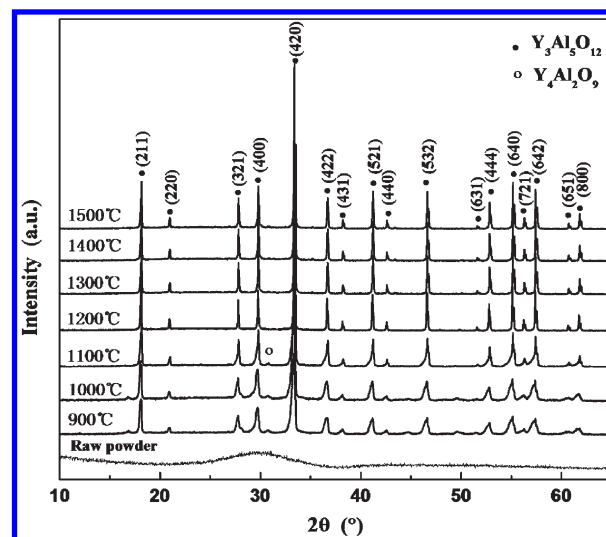

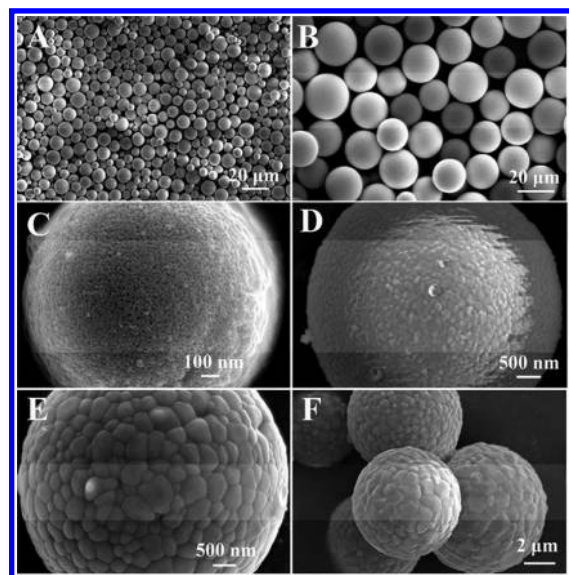**Figure 1.** XRD patterns of the raw powder and heat-treated samples.

(radius $\sim$5 μm) with a volume ratio of 1:5 and pressed into a thin pellet of thickness around 50 μm. Parts of the pellet were glued onto Cu slot grids and ion-beam milled to obtain electron-transparent areas with a 3 keV argon beam. The average diameter and standard size deviation of the crystallites were derived from 100 randomly selected crystallites with image analysis software. The volume particle size distribution of the powder sample was measured using a laser particle size analyzer (Mastersizer 2000, Malvern, U.K.) with a suitable Standard Operating Procedure (SOP) (refractive index, 1.78; vibration feed rate, 25%; measurement time, 30 s; dispersive air pressure, 1 bar). Thermal analysis measurements were performed using a differential scanning calorimeter DSC Q600 (TA Instruments) from room temperature to 1200 °C at different heating rates (5, 10, 20, and 40 K/min). Alumina pans were used as sample holders. The DSC measurements were carried out under a purified argon atmosphere using approximately 20 mg samples for all measurements. The photoluminescence excitation and emission spectra were recorded with a Hitachi F-4500 spectrophotometer equipped with a 60 W xenon lamp as the excitation source. The luminescent decay profiles were recorded on a steady state and fluorescence lifetime spectrometer (FLS920, Edinburgh Instrument).

3. RESULTS AND DISCUSSION

3.1. Phase Formation. Figure 1 shows the XRD patterns of the raw powder and heat-treated samples. It can be seen from the XRD pattern of the raw powder that there is a typical broad diffuse maximum, without a diffraction peak corresponding to a crystalline phase. Therefore, a glass powder with a YAG composition was successfully prepared by flame spraying—water quenching. When the glass powder was heat-treated at 900 °C, two phases crystallized from the amorphous particles. The dominant crystalline phase was a cubic $Y_3Al_5O_{12}$ phase with traces of monoclinic $Y_4Al_2O_9$. When the heat-treatment temperature increased to 1200 °C, the $Y_4Al_2O_9$ phase disappeared and a pure cubic $Y_3Al_5O_{12}$ was obtained. With the heat-treatment temperature further increased to 1500 °C, sharp and high diffraction peaks were observed. This might be associated with the grain growth of the YAG crystallite. The sizes of the $Y_3Al_5O_{12}$ crystallites have been estimated by using the Scherrer equation applied to the crystal plane of (420) at $2\theta = 33.400°$.[35] The $Y_3Al_5O_{12}$ crystallite sizes of the powder samples heat-treated at 900, 1000, and 1100 °C are 48, 65, and 85 nm, respectively.
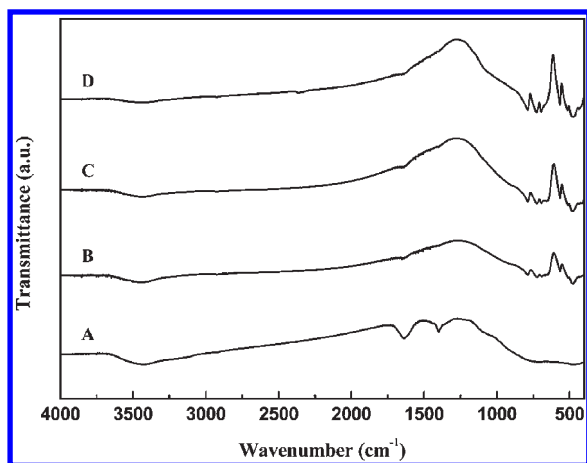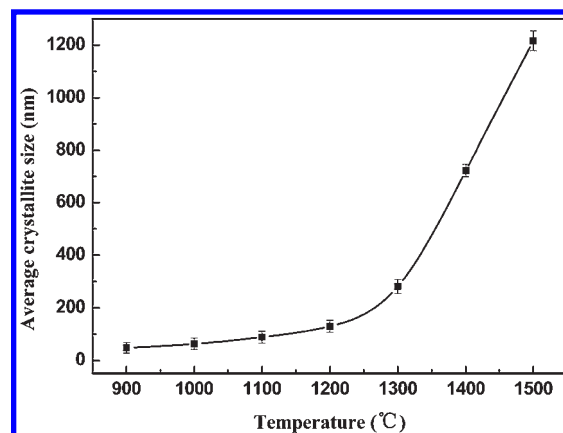
Figure 2. FTIR spectra of the glass powder (A) and powder samples heat-treated at 900 °C (B), 1200 °C (C), and 1500 °C (D).

Figure 4. Effect of heat-treatment temperature on the average size of the crystallites.

Figure 3. Low magnification SEM images of the glass powder derived from 660 L/h (A) and 400 L/h (B), and high magnification SEM images of the microspheres heat-treated at 900 (C), 1300 (D), 1400 (E), and 1500 °C (F).

Figure 2 shows the FTIR spectra of the glass powder and heat-treated samples. The broad peak of 3450 cm^{-1} can be assigned to the stretching vibrations of the O—H bond.[36] The peaks localized at 1636 and 1399 cm^{-1} are assigned to the asymmetrical and symmetrical stretching vibrations of the O—C=O bond, respectively.[36] These absorption peaks may be caused by the absorptions of H_2O and CO_2 in the synthesized powder and become weaker with the heat-treatment temperature increasing. When the glass powder was heat-treated at 900 °C, the characteristic absorption bands of YAG appear, in agreement with the result of XRD mentioned above. The peaks at about 790, 696, and 515 cm^{-1} represent the characteristic (Al—O) metal—oxygen vibrations, while the peaks at 729, 568, and 474 cm^{-1} represent the characteristic (Y—O) metal—oxygen vibrations.[37,38] With the increase of heat-treatment temperature, the shape of the peaks does not change except that the characteristic peaks become much sharper.

3.2. Morphology. The particle size of the glass powder was characterized by laser particle size analysis. To obtain glass powders with different sizes, the atomizing air flow rate operated in the spray-drying process was controlled. A high atomizing air flow rate often resulted in decreased spray droplet size as well as granule size.[39] The size of the end-products would indirectly be controlled by tunning the atomizing air flow rate. The particle sizes $D_{V,50}$ (volume median diameter) of the glass powders prepared by using granules spray-dried at atomizing air flow rates of 660 and 400 L/h are 10 and 22 μm, respectively.

Figure 3 shows the SEM images of the glass powder and heat-treated samples. The rapidly quenched glass powder is composed of regular microspheres, as shown in Figure 3A and B. The particle size of the glass microspheres is consistent with the results examined with a laser particle size analyzer. After being heat-treated, the spherical morphology and sizes of powder samples changed slightly. As seen from Figure 3C, the microsphere is actually composed of randomly aggregated crystallites. The average size of the crystallites determined from the SEM image is about 50 nm, which is in agreement with the XRD estimates. With increasing heat-treatment temperature, the average size of the crystallites grows to a bigger size, as shown in Figure 3D and E. When the heat-treatment temperature reaches 1500 °C, the average size of the crystallites grows to a micrometer size (1.2 μm), as shown in Figure 3F. The effect of the heat-treatment temperature on the average crystallite size determined from the SEM images is described in Figure 4. It can be seen that the average crystallite size is controlled on the nanometer scale (<100 nm) when the heat-treatment temperature is lower than 1100 °C. When the heat-treatment temperature increases to more than 1300 °C, the crystallites grow almost linearly with temperature. It is believed that the control of the crystallite size will have a great influence on the luminescence properties of the YAG:Ce^{3+} phosphor.

3.3. Crystallization Mechanism. The preparation of nano-/microstructured YAG:Ce^{3+} microspheres counts on crystallization of the rapidly quenched glass microspheres. Therefore, it is important to investigate the crystallization kinetics involved in the preparation process. The crystallization kinetics of the rapidly quenched glass microspheres were investigated by DSC under nonisothermal conditions.

The DSC traces for the rapidly quenched glass microspheres at different heating rates (5, 10, 20, and 40 K/min) are shown in
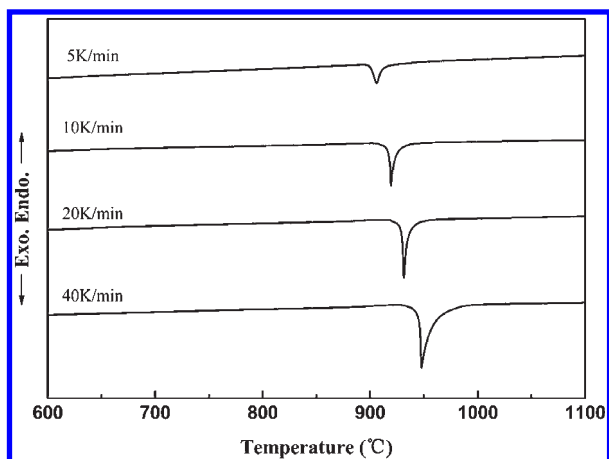
Figure 5. DSC traces for the glass microspheres at different heating rates.
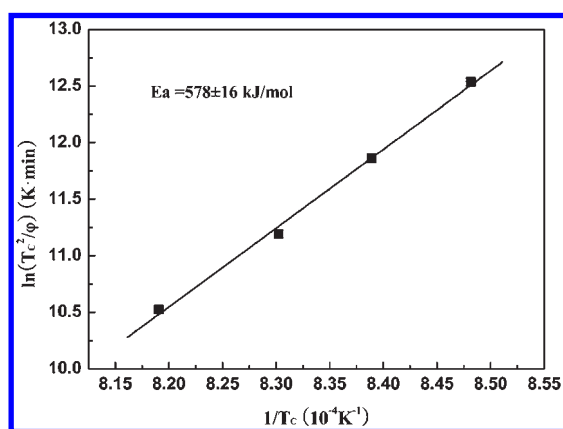
Figure 6. Kissinger plot for the exothermic crystallization peaks of the glass microspheres.

Figure 7. Optical microscope image of glass microspheres (A), SEM image of microspheres heat-treated at 800 °C (B), TEM image of a microsphere sample heat-treated at 900 °C (C), and SEM image of microspheres heat-treated at 1500 °C (D).

Figure 8. PL and PLE spectra of the YAG:Ce^{3+} microspheres.

Figure 5. The crystallization phenomenon induces a simple exothermic peak. The temperature of the crystallization peak (T_c) increases from 906 to 948 °C, when the heating rate increases from 5 to 40 K/min. The activation energy E_a for crystallization of the glass microspheres can be determined by the Kissinger equation:[40]
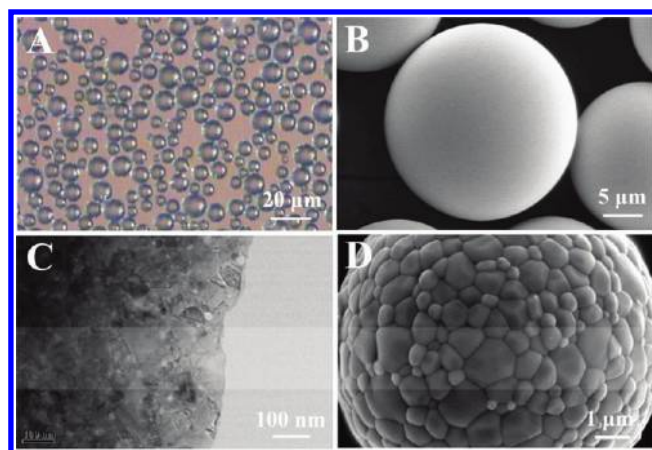
$$\ln\left(\frac{T_c^{\,2}}{\varphi}\right) = \frac{E_a}{RT_c} + C \qquad (1)$$

where T_c is the temperature of the DSC crystallization peak, φ is the heating rate, R is the universal gas constant, and C is a constant. The Kissinger plot for the exothermic crystallization peaks of the glass microspheres is shown in Figure 6. The value of the activation energy E_a for crystallization of the glass microspheres determined by the Kissinger equation is 578 ± 16 kJ/mol.
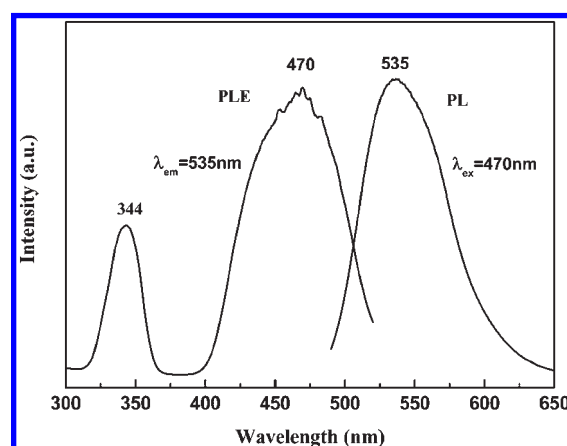
With the value of activation energy, the Avrami parameter n was calculated using a common method for nonisothermal analysis developed by Augis and Bennett:[40]

$$n = \frac{2.5}{\Delta T}\frac{RT_c^{\,2}}{E_a} \qquad (2)$$

where ΔT is the full width of the exothermic peak at the half-maximum intensity. The mechanism of the crystallization is correlated with the Avrami parameter n. Values of n close to 1 imply that surface crystallization dominates over all crystallization, values of n close to 2 imply two-dimension crystallization, values of 3 imply bulk crystallization, and values of 4 indicate homogeneous crystallization.[41] The Avrami parameter n for the 5, 10, 20, and 40 K/min DSC scans is 3.85 ± 0.10, 3.19 ± 0.09, 2.61 ± 0.07, and 1.79 ± 0.05, respectively. The errors on n are related to errors on E_a. This indicates that the crystallization mechanism changes from homogeneous crystallization to two-dimensional crystallization when the heating rate of the DSC scans increases from 5 to 40 K/min. Therefore, the powder samples prepared at a heating rate of 5 K/min should be associated with homogeneous crystallization.

The morphological evolution involved in the crystallization process is shown in Figure 7. It can be seen from Figure 7A that rapidly quenched glass microspheres, transparent as glass materials, usually perform. When they are heat-treated at a temperature below T_c, the microspheres maintain an amorphous state and show a smooth surface, as shown in Figure 7B. When the heat-treatment temperature is increased to T_c, crystallization takes place and a cubic garnet structure is rapidly formed in the volume of the microspheres, as shown in Figure 7C. With a further increase in heat-treatment temperature, the YAG crystallites grow to a bigger size, as shown in Figure 7D.

5358

dx.doi.org/10.1021/cg200939p |*Cryst. Growth Des.* 2011, 11, 5355–5361
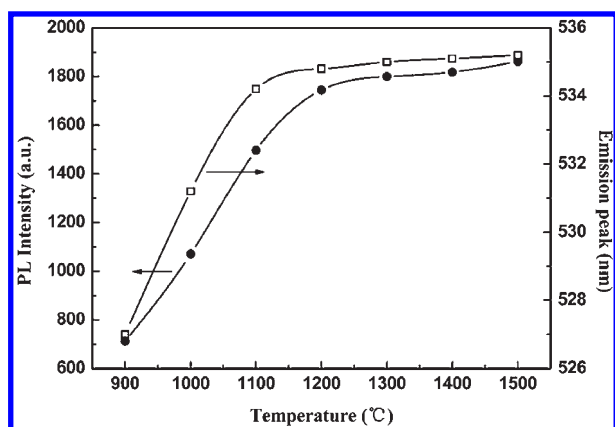
Figure 9. Effects of heat-treatment temperature on the PL intensity and emission peak.

Figure 10. Effect of the heat-treatment temperature on the luminescence decay curves of the YAG:Ce^{3+} microspheres.

3.4. Luminescence Properties. To fully explore the luminescence properties of the as-obtained nano-/microstructured YAG: Ce^{3+} microspheres, the photoluminescence (PL) and photoluminescence excitation (PLE) spectra, the luminescence decay curves, and the effects of heat-treatment temperature and different fluxes on luminescence properties were investigated in detail. The luminescence properties of the YAG:Ce^{3+} microspheres are characterized with the samples doped with 2.0 atom % Ce ions. Figure 8 shows the PL and PLE spectra of the YAG:Ce^{3+} microspheres (Figure 3F). The excitation peaks observed at 344 and 470 nm in the PLE spectra belong to the Ce^{3+} 4f-5d configuration. The emission consists of a peak at 535 nm and a shoulder at the longer wavelength side. The former is assigned to the 5d$^1 \rightarrow$ ^{2}F$_{5/2}$ transition and the latter to the 5d$^1 \rightarrow$ ^{2}F$_{7/2}$ transition, respectively, for Ce^{3+}, since Ce^{3+} with a 4f^1 electron configuration has two ground states of ^{2}F$_{5/2}$ and ^{2}F$_{7/2}$ due to the spin−orbit interaction.[42,43]

Figure 9 shows the effect of heat-treatment temperature on the PL intensity and emission peak. It can be seen that with increasing heat-treatment temperature the PL intensity increases almost linearly when the heat-treatment temperature is below 1200 °C. The greatly improved PL intensity is largely owing to the improved crystallinity of the host lattice. When the heat-treatment temperature further increases from 1200 to 1500 °C, the PL intensity exhibits only a slight enhancement, mainly due to further improved crystallinity and acquiring of a pure YAG phase, as revealed by the XRD patterns. It is evident that with increasing heat-treatment temperature the emission peak shows a red shift when the heat-treatment temperature is below 1100 °C. This might result from a lower crystal field effect of the nanocrystals crystallized from the glass microspheres at heat-treatment temperatures below 1100 °C, as revealed in Figure 4.[44] When the heat-treatment temperature increases to 1200 °C, the emission peak does not show any obvious changes.

Figure 10 shows the luminescence decay curve for the luminescence of Ce^{3+} (^{2}D$_{3/2}$ − ^{2}F$_{5/2}$) in YAG:Ce^{3+} microspheres. The decay curve can be fitted into a double exponential function as $I = A_1 \exp(-t/\tau_1) + A_2(-t/\tau_2)$, where A_1 and A_2 are constants and τ_1 and τ_2 are luminescence lifetimes. The long decay time τ_2 was the lifetime of the conventional emission, while the short lifetime τ_1 reflected the luminescence of Ce^{3+} on the surface.[45] Generally, the lifetime can be written as $\tau = (\gamma_r + \gamma_{nr})^{-1}$, where γ_r is the decay rate of the radiative process and γ_{nr} is the rate of the nonradiative process.[46] With increasing heat-treatment temperature, the content
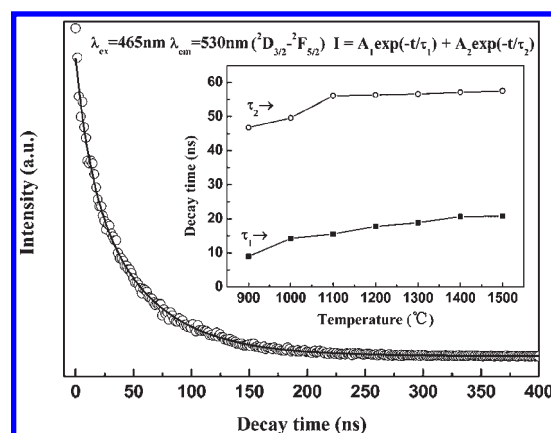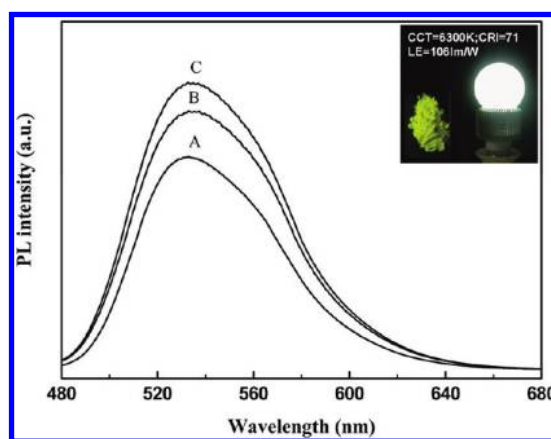
Figure 11. Emission spectra of the YAG:Ce^{3+} microspheres prepared without flux (A), with 1.0 wt % H$_3$BO$_3$ (B), or with 0.5 wt % H$_3$BO$_3$ + 0.5 wt % NaF (C).

of surface defects in the microspheres decreased, which usually act as quenching centers of luminescence. This is in agreement with the results of the FTIR. The decreased surface defects lead to a decreased nonradiative rate γ_{nr} and increased lifetime τ_1. The long lifetime τ_2 changes slightly at temperatures above 1100 °C, which indicates that the defects in the microspheres were almost eliminated by heat-treatment and the nonradiative rate γ_{nr} remained unchanged with elevated temperature.

In the process of phosphor production, fluxes such as H$_3$BO$_3$ and NaF were often used to improve the brightness of spherical shape phosphor particles.[47−49] Powder samples with the addition of different fluxes have been prepared by the controlled glass crystallization method. The fluxes were added into starting materials with the designed stoichiometric ratio, and other preparation conditions maintain unchanged. Figure 11 shows the effect of different fluxes on the PL intensity of the YAG:Ce^{3+} microspheres phosphor. It is obvious that the powder sample codoped with H$_3$BO$_3$ and NaF imposed a better effect than that of the single H$_3$BO$_3$ flux. The maximum PL intensity of the phosphor using 0.5 wt % H$_3$BO$_3$ and 0.5 wt % NaF fluxes was 135% of that the phosphor prepared without flux. This probably can be attributed to the improved crystallinity and local symmetry of the activator ions.[47,48] The YAG:Ce^{3+} microspheres prepared by the controlled glass crystallization method have been

5359

dx.doi.org/10.1021/cg200939p |*Cryst. Growth Des.* 2011, 11, 5355–5361

coated on a 470 nm InGaN blue LED to make a white LED lamp as shown in Figure 11. The correlated color temperature (CCT), color rendering index (CRI), and luminous efficacy (LE) of the white LED lamp at an operating current of 20 mA are 6300 K, 71, and 106 lm/W, respectively. The luminescence properties of the phosphor-converted white LED are comparable to those reported in the literature,[3,4] and they can be improved by further study.

4. CONCLUSIONS

In summary, nano-/microstructured YAG:Ce^{3+} microspheres have been successfully prepared by the controlled glass crystallization method. The heat-treatment temperature has an important influence on the structural and morphological evolution of $Y_3Al_5O_{12}$:Ce^{3+} microspheres. The heat-treated microspheres were composed of randomly aggregated crystallites, and their size can be tuned from nanometer scale to micrometer size by adjusting the heat-treatment temperature. The activation energy for crystallization of the glass microspheres determined by the Kissinger equation is 578 ± 16 kJ/mol. The crystallization mechanism for the $Y_3Al_5O_{12}$:Ce^{3+} microspheres has been proposed on homogeneous crystallization. The luminescence decay curve can be fitted into a double exponential function and the lifetime increased with increasing heat-treatment temperature. The maximum PL intensity of the phosphor using 0.5 wt % H_3BO_3 and 0.5 wt % NaF fluxes was 135% of that the phosphor prepared without flux. The color temperature, color rendering index, and luminous efficacy of the white LED packaged with the obtained YAG:Ce^{3+} microspheres are 6300 K, 71, and 106 lm/W, respectively.

■ AUTHOR INFORMATION

Corresponding Author
*Telephone: 86-10-82543695. Fax: 86-10-82543695. E-mail: ljt0012@vip.sina.com.

■ ACKNOWLEDGMENT

■ REFERENCES

(1) Schubert, E. F.; Kim, J. K. *Science* **2005**, *308*, 1274–1278.
(2) Pimputkar, S.; Speck, J. S.; DenBaars, S. P.; Nakamura, S. *Nat. Photonics* **2009**, *3*, 180–182.
(3) Ye, S.; Xiao, F.; Pan, Y. X.; Ma, Y. Y.; Zhang, Q. Y. *Mater. Sci. Eng., R* **2010**, *71*, 1–34.
(4) Im, W. B.; George, N.; Kurzman, J.; Brinkley, S.; Mikhailovsky, A.; Hu, J.; Chmelka, B. F.; DenBaars, S. P.; Seshadri, R. *Adv. Mater.* **2011**, *23*, 2300–2305.
(5) Li, Y. Q.; Hirosaki, N.; Xie, R. J.; Takeda, T.; Mitomo, M. *Chem. Mater.* **2008**, *20*, 6704–6714.
(6) Park, J. K.; Kim, C. H.; Park, S. H.; Park, H, D. *Appl. Phys. Lett.* **2004**, *84*, 1647–1649.
(7) Chan, T. S.; Liu, R. S.; Baginskiy, I. *Chem. Mater.* **2008**, *20*, 1215–1217.
(8) Im, W. B.; Fellows, N. N.; DenBaars, S. P.; Seshadri, R. *J. Mater. Chem.* **2009**, *19*, 1325–1330.
(9) Paulraj, A.; Natarajan, P.; Munnisamy, K.; Nagoor, M. K.; Nattar, K. P.; Abdulrazak, B.; Duraisamy, J. *J. Am. Ceram. Soc.* **2011**, *94*, 1627–1633.
(10) Li, J. G.; Li, X. D.; Sun, X. D.; Ishigaki, T. *J. Phys. Chem. C* **2008**, *112*, 11707–11716.
(11) Wang, L. S.; Zhou, Y. H.; Quan, Z. W.; Lin, J. *Mater. Lett.* **2005**, *59*, 1130–1133.
(12) Lee, S. H.; Koo, H. Y.; Jung, D. S.; Han, J. M.; Kang, Y. C. *Opt. Mater.* **2009**, *31*, 870–875.
(13) Kang, Y. C.; Chung, Y. S.; Park, S. B. *J. Am. Ceram. Soc.* **1999**, *82*, 2056–2060.
(14) Saxena, S. *Mater. Lett.* **2006**, *60*, 1315–1318.
(15) Pan, Y. X.; Wu, M. M.; Su, Q. *Mater. Sci. Eng., B* **2004**, *106*, 251–256.
(16) Peng, Y.; Xu, A. W.; Deng, B.; Antonietti, M.; Colfen, H. *J. Phys. Chem. B* **2006**, *110*, 2988–2993.
(17) Xu, A. W.; Antonietti, M.; Colfen, H.; Fang, Y. P. *Adv. Funct. Mater.* **2006**, *16*, 903–908.
(18) Yan, Y.; Wu, Q. S.; Li, L.; Ding, Y. P. *Cryst. Growth Des.* **2006**, *6*, 769–773.
(19) Xu, Z. H.; Kang, X. J.; Li, C. X.; Hou, Z. Y.; Zhang, C. M.; Yang, D. M.; Li, G. G.; Lin, J. *Inorg. Chem.* **2010**, *49*, 6706–6715.
(20) Lei, F.; Yan, B. *J. Phys. Chem. C* **2009**, *113*, 1074–1082.
(21) Devaraju, M. K.; Yin, S.; Sato, T. *Inorg. Chem.* **2011**, *50*, 4698–4704.
(22) Zhen, L.; Xu, C. Y.; Yang, L.; Shao, W. Z. *Cryst. Growth Des.* **2008**, *8*, 1734–1740.
(23) Sun, L. D.; Zhang, Y. X.; Zhang, J.; Yan, C. H.; Liao, C. S.; Lu, Y. Q. *Solid State Commun.* **2002**, *124*, 35–38.
(24) He, F.; Yang, P. P.; Wang, D.; Niu, N.; Gai, S. L.; Li, X. B. *Inorg. Chem.* **2011**, *50*, 4116–4124.
(25) Devaraju, M. K.; Yin, S.; Sato, T. *Cryst. Growth Des.* **2009**, *9*, 2944–2949.
(26) Li, X. X.; Hu, Z. G.; Li, J. T. *Opt. Mater.* **2007**, *29*, 854–857.
(27) Tan, C. B.; Liu, Y. X.; Han, Y. N.; Li, W. B. *J. Lumin.* **2011**, *131*, 1198–1202.
(28) Bras, W.; Clark, S. M.; Greaves, G. N.; Kunz, M.; Beek, W. V.; Radmilovic, V. *Cryst. Growth Des.* **2009**, *9*, 1297–1305.
(29) Chen, D. Q.; Yu, Y. L.; Wang, Y. S.; Huang, P.; Weng, F. Y. *J. Phys. Chem. C* **2009**, *113*, 6406–6410.
(30) Beall, G. H.; Duke, D. A. *J. Mater. Sci.* **1969**, *4*, 340–352.
(31) Tarafder, A.; Annapurna, K.; Chaliha, R. S.; Tiwari, V. S.; Gupta, P. K.; Karmakar, B. *J. Am. Ceram. Soc.* **2009**, *92*, 1934–1939.
(32) Cho, J. S.; Kang, Y. C. *Ceram. Int.* **2009**, *35*, 2103–2109.
(33) Weber, J. K. R.; Abadie, J. G.; Hixson, A. D.; Nordine, P. C.; Jerman, G. A. *J. Am. Ceram. Soc.* **2000**, *83*, 1868–1872.
(34) Rosenflanz, A.; Frey, M.; Endres, B.; Anderson, T.; Richards, E.; Schardt, C. *Nature* **2004**, *430*, 761–764.
(35) Zhang, Y. W.; Jin, S.; Tian, S. J.; Li, G. B.; Jia, T.; Liao, C. S.; Yan, C. H. *Chem. Mater.* **2001**, *13*, 372–378.
(36) Fagui, Q.; Xipeng, P.; Xuejian, L.; Yubai, P.; Jingkun, G. *Ceram. Int.* **2005**, *31*, 663–665.
(37) Bhattacharyya, S.; Ghatak, S. *Ceram. Interfaces* **2009**, *35*, 29–34.
(38) Yenpei, F. *J. Alloys Compd.* **2006**, *414*, 181–185.
(39) Behzadi, S. S.; Prakasvudhisarn, C.; Klocker, J.; Wolschann, P.; Viernstein, H. *Powder Technol.* **2009**, *195*, 150–157.
(40) Nascimento, M. L. F.; Dantas, N. O. *Mater. Lett.* **2007**, *61*, 912–916.
(41) Hu, A. M.; Liang, K. M.; Zhou, F.; Wang, G. L.; Peng, F. *Ceram. Interfaces* **2005**, *31*, 11–14.
(42) Kasuya, R.; Isobe, T.; Kuma, H.; Katano, J. *J. Phys. Chem. B* **2005**, *109*, 22126–22130.
(43) Kasuya, R.; Kawano, A.; Isobe, T. *Appl. Phys. Lett.* **2007**, *91*, 111916–111918.
(44) Jia, D. D.; Wang, Y.; Guo, X.; Li, K.; Zou, Y. K.; Jia, W. Y. *J. Electrochem. Soc.* **2007**, *154*, J1–J4.
(45) Zhang, W. W.; Zhang, W. P.; Xie, P. B.; Yin, M.; Chen, H. T.; Jing, L.; Zhang, Y. S.; Lou, L. R.; Xia, S. D. *J. Colloid Interface Sci.* **2003**, *262*, 588–593.
(46) Zhang, K.; Hu, W. B.; Wu, Y. T.; Liu, H. Z. *Inorg. Mater.* **2008**, *44*, 1218–1223.

(47) Xu, S. Q.; Sun, L. Z.; Zhang, Y.; Ju, H. D.; Zhao, S. L.; Deng, D. G.; Wang, H. P.; Wang, B. L. *J. Rare Earth* **2009**, *27*, 327–329.

(48) Zhou, J.; Wang, Y.; Liu, B.; Lu, Y. H. *J. Alloys Compd.* **2009**, *484*, 439–443.

(49) Lee, S. H.; Koo, H. Y.; Jung, D. S.; Han, J. M.; Kang, Y. C. *Opt. Mater.* **2009**, *31*, 870–875.

5361

dx.doi.org/10.1021/cg200939p |*Cryst. Growth Des.* 2011, 11, 5355–5361